We are IntechOpen, the world's leading publisher of Open Access books Built by scientists, for scientists

4,800
Open access books available

122,000
International authors and editors

135M
Downloads

Our authors are among the

154
Countries delivered to

TOP 1%
most cited scientists

12.2%
Contributors from top 500 universities

WEB OF SCIENCE™

Selection of our books indexed in the Book Citation Index in Web of Science™ Core Collection (BKCI)

Interested in publishing with us?
Contact book.department@intechopen.com

Numbers displayed above are based on latest data collected.
For more information visit www.intechopen.com

Chapter 13

Gain Saturation in Optical Fiber Laser Amplifiers

Maryam Eilchi and Parviz Parvin

Additional information is available at the end of the chapter

http://dx.doi.org/10.5772/62136

Abstract

This chapter describes the determination of amplifying parameters in rare–earth–doped optical fiber laser amplifiers. In the context of this review, the system will be analyzed under both continuous–wave (CW) and pulse conditions. A comprehensive analysis has been implemented using the set of coupled propagation rate equations based on the atomic energy structure of dopant as well as the absorption and emission cross sections.

Regarding the spectral line broadening associated with a suitable amplification relation, gain and saturation can be acquired for various pumping schemes including co– or counter–propagation and the bidirectional modes.

It was shown that the gain and saturation properties are strongly dependent on the pump power, dopant concentration, and fiber length mainly due to the dominant effect of the overlapping factor of dual–clad fibers.

Keywords: Gain, Saturation, ASE parasitic noises, Broadening, Amplification relation, Filling (overlapping) factor

1. Introduction

Recently, intense activities have been devoted to characterize rare–earth–doped double–clad fiber laser amplifiers. Owing to their compactness, superb beam quality, great thermal control, and high efficiency, they demonstrate to be important light sources in medicine, modern telecommunication [1], and industries [2, 3]. Progress has been made in developing a fiber–based source in which the mean power scales up to several kilowatts.

The purpose of the fiber amplifier is to intensify a less powerful optical beam, which propagates either inside another fiber or in free space. In this way, the amplifier is "seeded" with a low–power laser beam. As it is known from the main principles of laser physics, the laser oscillator

is a device that contains an optical amplifier and puts inside a resonator to provide positive feedback.

The fiber amplifiers are fundamentally divided into core–pumped and cladding–pumped [4] according to the environment of the pump propagation. In the former classification, the amplifying light propagates in the same volume where laser gain media is located, while in the latter, the pump is coupled and propagates outside the core of the doped fiber. The same classification is valid for fiber laser oscillators. Cladding–pumped amplification technique is a hot topic in laser science and technology for high–power regimes, which is the focus of this chapter.

After the invention of the dual–clad fibers, the output powers of the doped fiber lasers have been lifted by several orders of magnitude, and immense activities have been devoted to relevant topics. These systems demonstrate several inherent features including [5] non–uniformly distributed population inversion due to end pumping as well as very high gain even in single–pass amplification by a large ratio of gain length to cross–sectional area.

In addition, both neodymium (Nd) and ytterbium (Yb) are suitable doping elements for high–power regime. Despite the fact that Nd has a relatively low laser threshold, Yb–doped double–clad fiber amplifiers present the prospects for a number of interesting applications due to the broad gain bandwidth with excellent beam quality, renowned as potential sources accessible to high–pump absorption, leading to ultimate efficiency [5, 6]. Furthermore, the benefits from efficient performance, small quantum defects, and superb spectroscopic characteristics as well as free competition processes are competitive with other rare–earth dopants. Particularly, the capability of generating high powers makes them very attractive wherein the output power up to 10/50 kW at CW single–mode/multi–mode schemes has been recently reported.

Besides, a fiber amplifier is characterized by a couple of significant coefficients, i.e., the small signal gain and the saturation quantity. In this chapter, a theoretical consideration of the CW and pulsed fiber arrays is reviewed, followed by the derived main formulas that are important for practical design. In Section 2, a brief description has been devoted to various types of laser amplifiers, operating based on the stimulated emission and optical nonlinearities. An extensive analysis is given in Section 3, regarding the set of coupled propagation rate equations accompanied with the effect of amplified spontaneous emission (ASE) parasitic noises for various pumping modes based on the atomic energy structure of dopants. The serious spectral line broadening mechanisms of gain media is described in Section 4. Eventually, the main issue of relevant amplification relation has been investigated in order to find the corresponding gain saturation parameters.

2. Various types of fiber laser amplifiers

Different kinds of laser amplifiers operate based on the stimulated emission amplification principle, or established upon optical nonlinearities, e.g., Raman or Brillouin amplifiers as well as optical parametric amplifiers (OPAs).

Raman–based fiber laser amplifier is one approach that has attracted several groups [7–13]. Here, the governed amplification process is the stimulated Raman scattering (SRS) in the fiber which causes an energy transfer from the pump to the signal. In fact, the vibrational spectrum of core material defines the Raman shift. If the wavelength of laser beam signal is known, then the optimum wavelength for pump signal can be calculated.

Commonly, Raman fiber lasers and amplifiers are not considered as ways for generating high–power narrow–linewidth lasers. For high–efficient operations, typically hundreds of meters of fiber are necessary to provide enough gain.

On the contrary, the optical gain is obtained by stimulated Brillouin scattering (SBS) in the Brillouin fiber amplifiers. It is also pumped optically, and a part of the pump power is transmitted to the signal through SBS. Physically, each pump photon creates a signal photon, and the remaining energy is used to excite an acoustic phonon [14]. Classically, the pump beam gets scattered from an acoustic wave moving through the medium at the speed of sound.

Moreover, the fiber–based OPA is a well–known technique offering a wide gain bandwidth using only a few hundred meters of fiber [15]. This phenomenon is strictly operated based on four–wave mixing (FWM) and phase–matching nonlinearities [16] in which a couple of interacting photons over two wavelength bands, also called pump and idler, usually travel collinearly through a nonlinear optical crystal, creating signal and idler output photons. During this phenomenon, pump light beam becomes weaker and amplifies the idler wave.

For birefringent nonlinear crystals, the collinear incident beams may non–collinearly scatter outside the crystal. Non–collinear OPAs were developed to have additional degree of freedom for central wavelength selection, allowing constant gain up to second order in wavelength.

3. Theory

3.1. Absorption and emission cross sections

All rare–earth–doped fiber amplifiers intensify the seed signal light through stimulated emission. The local rate equations describe the dynamics of the emission and absorption processes of doping ions within its host material by making use of its atomic energy structure as well as spectroscopic properties [17]. The relation between the emission and absorption cross sections for two energy–level gain media is determined using McCumber theory, which satisfies the following formula [18]:

$$\sigma_{\mathrm{e}}(\nu) = \sigma_{\mathrm{a}}(\nu)\exp\left(\frac{\varepsilon(T) - h\nu}{K_{\mathrm{B}}T}\right) \tag{1}$$

where σ_{a} and σ_{e} are the absorption and emission cross sections, h, ν, K_B, and T depict the Planck constant, frequency of light, Boltzmann constant, and the absolute temperature in

Kelvin, respectively. Moreover, $\varepsilon(T)$ shows the mean transition energy between two manifolds at temperature T. This quantity, which depends on the temperature but not on the optical frequency, can be calculated from the energies of the single Stark levels. Otherwise, one can obtain an estimation regarding the assumption that the energy levels within each Stark manifold are equidistant [19]. Alternatively, $\varepsilon(T)$ can be calibrated, e.g., using the reciprocity method or the Füchtbauer–Ladenburg equation. On the contrary,

$$\exp\left(\frac{\varepsilon(T)}{K_B T}\right) = \frac{Z_1}{Z_2}\exp\left(\frac{E_2 - E_1}{K_B T}\right) \tag{2}$$

where Z_1 and Z_2 are the partition functions, and E_1 (E_2) is the first (second) energy level. For Yb–doped gain mediums, $\varepsilon(T)$ is often close to the photon energy of the zero–phonon transition, i.e., the transition between the lowest sublevels of both manifolds. Furthermore, at λ=975 nm, $\varepsilon(T)=h\nu$ becomes equal to 1.27 eV, which leads to $\sigma_e=\sigma_a$. An additional formula is provided by the McCumber analysis, linking the radiative lifetime and the emission cross section as follows:

$$\frac{1}{\tau} = \frac{8\pi n^2}{C^2}\int \nu^2 \sigma_e(\nu) d\nu \tag{3}$$

Here, τ indicates the lifetime of the excited state level of atoms, n is the refractive index of the gain media, and C denotes the speed of light in vacuum. As an example, Figure 1 demonstrates a model for the Yb^{3+} ions energy–level structure, consisting of two manifolds: a ground state $^2F_{7/2}$ (with four Stark levels labeled L_0, L_1, L_2, and L_3) and a well–separated excited state $^2F_{5/2}$ (with three Stark levels labeled U_0, U_1, and U_2), which is seated ~10000 cm^{-1} above the ground level. This is the reason why there is no excited state absorption (ESA) at either the pump or laser wavelengths [6]. This large energy gap also precludes the concentration quenching and the nonradiative decay via multiphonon emission from $^2F_{5/2}$ even in a host of high phonon energy such as silica. The energy band diagram for the lasing material is a quasi–three–level system [20].

The first transition between two Yb manifolds is the absorption and emission of the pump. Afterward, the spontaneous decay from the $^2F_{5/2}$ manifold, as well as the absorption, and stimulated emission of the signal simultaneously appear.

Absorption and stimulated emission cross sections of Yb–doped silica glass optical fibers are shown in the spectroscopic diagram in Figure 2. The absorption or fluorescence peak at 975 nm (A) represents the zero–line transition between the lowest energy levels of the ground state (L_0) and the excited state (U_0) in the manifold. The laser operation at 975 nm is a three–level process because the emission is due to a transition to the lowest Stark level. The absorption peak at shorter wavelength (B) corresponds to a transition from the ground level L_0 to either of the excited level U_1 and U_2. The absorption peak at longer wavelength (C) is attributed to

http://dx.doi.org/10.5772/62136

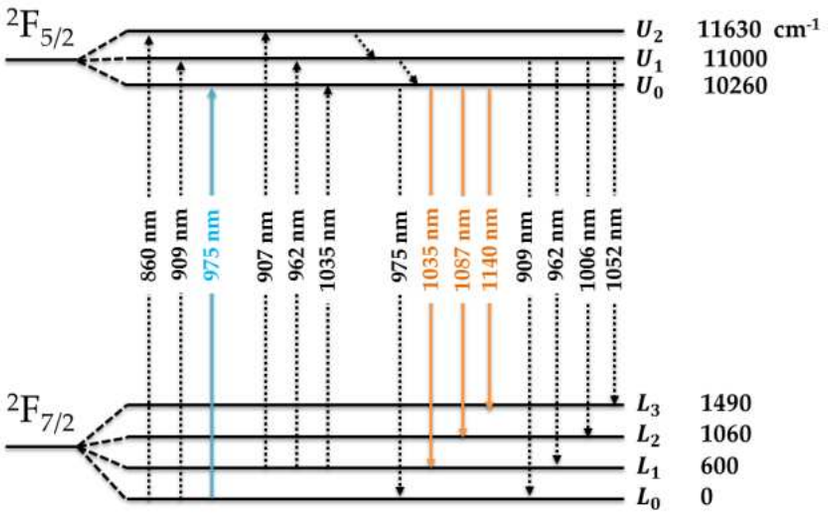

Figure 1. Energy–level diagram of Yb:silica glass

the transition from level L_1 which can produce reabsorption and leads to higher thresholds in the Yb^{3+} laser systems working around 1 μm.

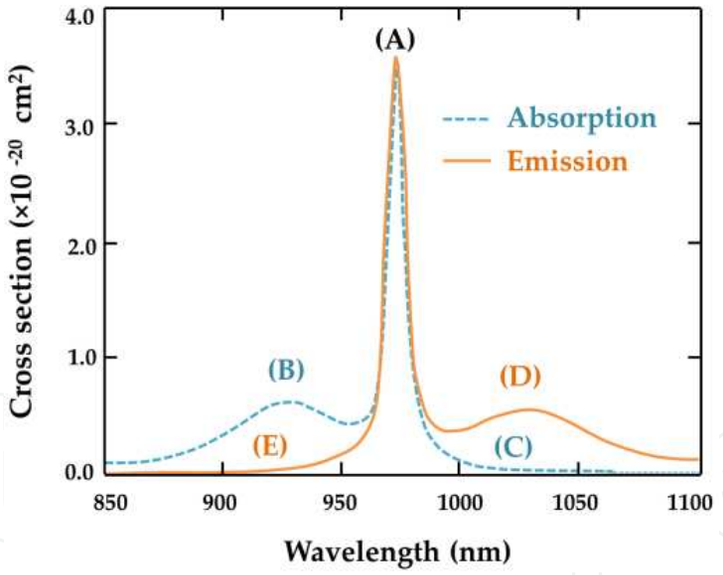

Figure 2. Typical absorption and emission spectra of Yb^{3+} ions in germanosilicate host [21]

In addition, the emission spectrum peak (D) corresponds to the energy transfer from level U_0 to the levels L_1, L_2, and L_3, while that at (E) belongs to the transition from level U_1, generating weak emissions around 900 nm. The broad absorption spectrum of Yb^{3+} ions enables the easy configuration of the pump wavelength. Depending on the requirement of the laser system, the laser signal wavelength can be configured in the range from 970 nm to 1200 nm due to the wide emission spectrum of Yb.

3.2. Rate equations

Amplifier characteristics, comprising the operating wavelength and the gain bandwidth, are determined by the dopants rather than by the host medium. However, because of the tight confinement of light provided by guided modes, fiber amplifiers can provide high optical gains at moderate pump intensity levels over relatively large spectral bandwidths, making them suitable for many telecommunications and signal–processing applications [22].

Currently, the rate equations are known as the most powerful tools to foresee the laser amplifier features associated with the non–uniform pumping along the laser length [23–31]. Here, the rate equations for the quasi–three–energy–level structures are typically introduced with the definition of the relevant parameters. Using the fourth–order Runge–Kutta method, the effect of ASE parasitic noises and gain can be considered to assess the efficiency. The performance of amplifiers also depends on the rates of radiative and nonradiative decays caused by several mechanisms related to lattice vibrations, ion–ion interactions, and cooperative up–conversion to higher levels [32].

In the case of fiber amplifier as a single–pass array without reflectors, the backward signal intensity, $I^{-}(z, t, \lambda)$, is equal to zero. Therefore, the set of coupled propagation rate equations accompanied with ASE in the pulsed regime can be organized as follows [33–35]:

$$\begin{aligned}\frac{\partial N_2(z,t,\lambda)}{\partial t} &= \frac{\Gamma_p(\lambda)\lambda_p}{hC}\left[\sigma_{ap}(\lambda)N - \sigma_p^{tot}(\lambda)N_2(z,t,\lambda)\right]I_p^{tot}(z,t,\lambda)\\ &+\frac{1}{hC}.\sum_j \Gamma_A(\lambda_j)\lambda_j\left[\sigma_{aA}(\lambda_j)N - \sigma_A^{tot}(\lambda_j)N_2(z,t,\lambda_j)\right]I_A^{tot}(z,t,\lambda_j)\\ &+\frac{\Gamma_s(\lambda)}{hC}\int\left[\sigma_a(\lambda)N - \sigma^{tot}(\lambda)N_2(z,t,\lambda)\right]I^{+}(z,t,\lambda)\lambda d\lambda - \frac{N_2(z,t,\lambda)}{\tau} - C_{up}N_2^2(z,t,\lambda)\end{aligned} \tag{4}$$

$$\pm\frac{dI_p^{\pm}(z,t,\lambda)}{dz} = \pm\Gamma_p(\lambda)\left[\left\{\sigma_p^{tot}(\lambda) - \sigma_{24}(\lambda)\right\}N_2(z,t,\lambda) - \sigma_{ap}(\lambda)N\right]I_p^{\pm}(z,t,\lambda) \mp \alpha_p I_p^{\pm}(z,t,\lambda) \tag{5}$$

$$\frac{dI^{+}(z,t,\lambda)}{dz} = \Gamma_s(\lambda)\left[\sigma^{tot}(\lambda)N_2(z,t,\lambda) - \sigma_a(\lambda)N\right]I^{+}(z,t,\lambda) - \alpha_s I^{+}(z,t,\lambda) \tag{6}$$

$$\begin{aligned}\pm\frac{dI_A^{\pm}(z,t,\lambda_j)}{dz} &= \pm\Gamma_A(\lambda_j)\left[\sigma_A^{tot}(\lambda_j)N_2(z,t,\lambda_j) - \sigma_{aA}(\lambda_j)N\right]I_A^{\pm}(z,t,\lambda_j)\\ \mp\alpha_A I_A^{\pm}(z,t,\lambda_j) &\pm \Gamma_A(\lambda_j)\sigma_{eA}(\lambda_j)N_2(z,t,\lambda_j)I_0(\lambda) \pm S.\alpha_{RS}(\lambda)I_A^{\mp}(z,t,\lambda_j)\end{aligned} \tag{7}$$

where the superscripts "±" describe the traveling directions of the light waves along the fiber propagation axis (z). Furthermore, p, s, and A subscript indexes define the parameters at the

pump, laser, and ASE wavelengths. The notation I denotes the intensity of the pump, lasing, or ASE radiations, and $I^{tot}(z, t, \lambda)$, which stands for the total intensity, is the summation of forward, $I^{+}(z, t, \lambda)$, and backward, $I^{-}(z, t, \lambda)$, beams. Hence, some pumping modes are considered, including co–propagation, since both the signal and pump intensities are injected at $z=0$ and propagate in the same direction or counter–propagation since the pump intensity is entered at $z=L$ (the signal and pump propagate in the opposite directions). When the pump injects in both fiber ends, it results in the bidirectional configuration.

Furthermore, $N_1(z, t, \lambda)$ and $N_2(z, t, \lambda)$ represent the population of the ground state as well as the upper lasing level of atoms, accordingly. $N(z, t, \lambda)=N_1(z, t, \lambda)+N_2(z, t, \lambda)$ describes the dopant concentration per unit volume, σ^{tot} is equal to $(\sigma_a+\sigma_e)$, and λ is the wavelength of the light. The absorption of excited state level at the pump wavelength is indicated by σ_{24} which is independent on the population of the upper level of laser.

In order to solve these equations, the cooperative up–conversion coefficient (C_{up}) must be known. According to the model mentioned in [36], it can be expressed as

$$C_{up}=\frac{4\pi}{3}\frac{R_0^6}{R^3\tau} \tag{8}$$

where R shows the average separation between various uniformly distributed ions, R_0 demonstrates a critical interaction distance, and $\tau=1/A_{21}$. Neglecting the formation of ion pairs, we can approximately consider

$$R_0^6=\frac{9}{16\pi^2}\frac{C_{up}\tau}{N_{\text{doped ions}}} \tag{9}$$

On the contrary, the local intensity per unit wavelength, $I_0(\lambda)\cong 2mhC^2(1/A_{core})\Delta\lambda_s/\lambda_s^3$ [37], is a constant parameter accounting for the contribution of the spontaneous emission into the propagating single transverse laser mode with the spectral bandwidth $\Delta\lambda$, where the factor two arises from a couple of orthogonal polarization directions. The parameter m exhibits the number of transverse modes inside the fiber which is unity for monomode fibers.

In low–power communication fiber amplifiers, the core and cladding structures are centro-symmetric having circular cross sections. In order to remove this power limitation, an intelligent solution was proposed in 1988 by Snitzer and coworkers, namely double–clad fibers. At this model, the fiber core is off–centered or the inner cladding form is triangular, rectangular, hexagonal, elliptical, D–shaped, and so on, where the rays scatter in many accessible directions [25, 38, 39]. Hereupon, the pump light helically propagates through the clad and interacts with the active core. The pump overlapping factor (Γ_p) states that how much of the pump mode intensity actually coupled to the gain media. Assuming a spatially uniform pump distribution over the inner clad cross section, Γ_p can be estimated approximately by

$$\Gamma_p(\lambda) = \int_0^{2\pi}\int_0^a \Gamma_p(r,\varphi,\lambda) r dr d\varphi = \int_0^{2\pi}\int_0^a \frac{r dr d\varphi}{A_{clad}} \cong \frac{A_{core}}{A_{clad}} \tag{10}$$

where a stands for the core radius of active fiber and A_{core} and A_{clad} for the mode field area of the core and the multimode first cladding, respectively. On the contrary, the signal filling factor provides a figure of interaction between the optical modes at the signal radiation and the dopant ions profile. The spatial overlap integral due to the signal indicates that [25, 40, 41]

$$\Gamma_s(\lambda) = \int_0^{2\pi}\int_0^a \Gamma_s(r,\varphi,\lambda) r dr d\varphi = \int_0^{2\pi}\int_0^a \frac{\psi(r,\varphi,\lambda) r dr d\varphi}{\int_0^{2\pi}\int_0^{\infty}\psi(r,\varphi,\lambda) r dr d\varphi} = \frac{I^{core}}{I^{core} + I^{clad}} \tag{11}$$

For single–clad fibers, the dimensionless coefficient $\Gamma_s(\lambda)$ is equal to unity, while it is smaller than unity (0.6–0.86) in double–clad fibers. Apparently, Γ_s is a function of the pump intensity which approaches a saturated value at high pumping rates [42]. Furthermore, I^{core} and I^{clad} are defined as the intensity confined in the core and inner cladding, respectively [25], which can be theoretically expressed as follows [41]:

$$I^{core} = \frac{1}{A_{core}}\int_0^a J^2\left[U(r/a)\right] J^{-2}(U) r dr \tag{12}$$

$$I^{clad} = \frac{1}{A_{core}}\int_a^{\infty} K^2\left[W(r/a)\right] K^{-2}(W) r dr \tag{13}$$

Here, $\psi(r, \varphi, \lambda)$ shows the normalized transverse envelope of the modal field intensity, and $J(K)$ demonstrates the Bessel function (modified Bessel function) inside (outside) the fiber core. Parameters U and W are determined by the characteristic equations that satisfy the boundary conditions at $r = a$, namely [43]:

$$U = a\sqrt{n_{core}^2 k_0^2 - \beta^2} \tag{14}$$

$$W = a\sqrt{\beta^2 - n_{clad}^2 k_0^2} \tag{15}$$

where n_{core} and n_{clad} denote the refractive indices of the fiber core and inner cladding, respectively. The propagation constant β of any mode of fiber is limited within the interval $n_{core}k_0 \geq \beta \geq n_{clad}k_0$ which can be defined as $\beta = n_{eff}k_0$. In this equation, n_{eff} is the effective refractive

index and $k_0=2\pi/\lambda_0$ is the wave number in free space. The intensity profile $|\psi(r, \varphi, \lambda)|^2$ resembles the linearly polarized $L\ P_{lm}$ modes. In terms of normalized electromagnetic field distribution of the fiber [44], we find that

$$\int_0^{2\pi}\int_0^{\infty}\psi\left(r,\varphi,\lambda\right)rdrd\varphi = Re\left[\int_0^{2\pi}\int_0^{\infty}E\left(r,\varphi,\lambda\right)\times H^{*}\left(r,\varphi,\lambda\right).\hat{z}\ rdrd\varphi\right]=1 \tag{16}$$

where E and H depict the electric and magnet fields of the propagation mode, respectively, and the versor of the z propagation direction is indicated by $\hat{z}$. In the case of a Gaussian envelope approximation [45], the distribution of signal overlapping factor is as follows:

$$\Gamma_s\left(\lambda\right)\cong 1-\exp\left[-2\left(\frac{b}{\omega_s\left(\lambda\right)}\right)^2\right] \tag{17}$$

where b shows the radius of doped area, and $\omega_s(\lambda)$ is $1/e^2$ of the intensity profile radius at the given wavelength calculated from the polynomial form [46]:

$$\omega_s\left(\lambda\right)=a\left[A_1+A_2/V^{1.5}\left(\lambda\right)+A_3/V^{6}\left(\lambda\right)\right] \tag{18}$$

On the one hand, the normalized frequency is defined as $V=2\pi a.NA/\lambda_s$, where NA represents the corresponding numerical aperture. For single–mode fibers, V could be smaller than 2.405 which hints that the core supports only the fundamental transverse $L\ P_{01}$ mode.

On the other hand, along with the signal, the spontaneous emission is also intensified. In fact, the parasitic ASE noises cause the degradation of the signal–to–noise ratio (SNR) [47–49]. It is due to the lack of reflectors such as fiber Bragg gratins (FBGs) or dichroic mirrors in the amplifier stage, while the selective wavelength oscillates in the oscillator. The evolution formula for the ASE intensities propagating in a given direction is written according to Eq. (7). The total ASE noise at point z along the fiber is the consequence of the intensity of ASE from the previous sections of the fiber accompanying the local intensity $I_0(\lambda)$ due to spontaneous emission. The modified population inversion deals with the ASE terms too.

The positive scattering parameter $\alpha_{RS}(\lambda)=B/\lambda^4$ includes the losses due to Rayleigh scattering. The Rayleigh scattering coefficient B of pure silica is found to be ~0.63 dBμm^4/km, and S denotes the capture fraction by the fiber, such that a fraction $S.\alpha_{RS}(\lambda)=1.3\times10^{-7}\text{m}^{-1}$ [50] is recaptured by the fiber. The capture fraction is defined as the proportion of the total energy scattered at z which is recaptured by the fiber in the return direction that increases with $(NA)^2$ [48, 51, 52].

In addition, Γ_A is defined as ASE filling factor which arises from the interaction between ASE modes and core dopant concentration, and α_A displays the ASE scattering loss. For simplicity, Γ_A and α_A for various ASE peaks presume to be identical to the main signal in the vicinity of λ_s. The ASE spectrum is divided into several channels with spectral width $\Delta\lambda$, whereas the signal channel width $\Delta\lambda_s$ is much smaller than the former, i.e., $\Delta\lambda_s \ll \Delta\lambda$. The ASE intensities $I_A^{\pm}(z, t, \lambda_j)$ actually propagate in the positive and the negative z –directions, both in co– and counter-propagation with the signal. Hence, the total ASE parasitic noise is stated by introducing forward and backward ASE components at any point of the fiber, namely

$$I_A^{tot}\left(z,t,\lambda_j\right) = I_A^{+}\left(z,t,\lambda_j\right) + I_A^{-}\left(z,t,\lambda_j\right) \tag{19}$$

It is worth noting that the boundary conditions for the ASE channels are given by $I_A^{+}(0) = I_A^{-}(L) = 0$.

Furthermore, Rayleigh backscattering (RBS) is another important issue that affects the performance of the signal source, unless the optical isolators are well employed [48, 49, 53]. When ASE and RBS are intense enough, these may restrict the amplifier gain leading to a drop in the efficiency in many applications. In the case of strongly pumped condition, RBS at the ASE wavelengths can be ignored mainly due to the reduction of ASE to get significantly weaker than the signal [54]. Here, we assume that

$$I^{\pm}\left(z,t,\lambda\right) \cong I_s^{\pm}\left(z,t\right)\delta\left(\lambda-\lambda_s\right) \tag{20}$$

$$\frac{dI^{\pm}\left(z,t\right)}{dz} \equiv \frac{\partial I^{\pm}\left(z\right)}{\partial z} \pm \frac{n}{C}\frac{\partial I^{\pm}\left(t\right)}{\partial t} \tag{21}$$

Thus, the rate equations at signal wavelength can be simplified as follows:

$$\begin{aligned}\frac{\partial N_2\left(z,t\right)}{\partial t} &= \frac{\Gamma_p\lambda_p}{hC}.\left[\sigma_{ap}N - \sigma_p^{tot}N_2\left(z,t\right)\right]I_p^{tot}\left(z,t\right) + \\ &+ \frac{1}{hC}.\sum_j \Gamma_A\lambda_j\left[\sigma_{aA}(\lambda_j)N - \sigma_A^{tot}N_2\left(z,t\right)\right]I_A^{tot}\left(z,t\right) + \\ &+ \frac{\Gamma_s\lambda_s}{hC}\left[\sigma_{as}N - \sigma_s^{tot}N_2\left(z,t\right)\right]I_s^{+}\left(z,t\right) - \frac{N_2\left(z,t\right)}{\tau} - C_{up}N_2^2\left(z,t\right)\end{aligned} \tag{22}$$

$$\frac{\partial I_p^{\pm}\left(z\right)}{\partial z} \pm \frac{n}{c}\frac{\partial I_p^{\pm}\left(t\right)}{\partial t} = \pm\Gamma_p\left[\left(\sigma_p^{tot}-\sigma_{24}\right)N_2\left(z,t\right) - \sigma_{ap}N\right]I_p^{\pm}\left(z,t\right) \mp \alpha_p I_p^{\pm}\left(z,t\right) \tag{23}$$

$$\frac{\partial I_s^+(z)}{\partial z} \pm \frac{n}{c}\frac{\partial I_s^+(t)}{\partial t} = \Gamma_s\left[\sigma_s^{tot}N_2(z,t) - \sigma_{as}N\right]I_s^+(z,t) - \alpha_s I_s^+(z,t) \tag{24}$$

$$\begin{aligned}&\frac{\partial I_A^\pm(z)}{\partial z} \pm \frac{n}{c}\frac{\partial I_A^\pm(t)}{\partial t} = \pm\Gamma_A\left[\sigma_A^{tot}N_2(z,t) - \sigma_{aA}N\right]I_A^\pm(z,t)\\ &\mp\alpha_A I_A^\pm(z,t) \pm \Gamma_A\sigma_{eA}N_2(z,t)I_0(\lambda) \pm S.\alpha_{RS}(\lambda)I_A^\mp(z,t)\end{aligned} \tag{25}$$

However, in the case of CW fiber amplifiers, disregarding ESA and cooperative up–conversion, the set of first–order coupled nonlinear time–independent steady–state ($\partial/\partial t \rightarrow 0$) differential equations of an end–pumped configuration is realized by [28, 34, 37]

$$\frac{N_2(z)}{N} = \frac{\Gamma_p\lambda_p\sigma_{ap}P_p^{tot}(z) + \sum_j\Gamma_A\lambda_j\sigma_{aA}(\lambda_j)P_A^{tot}(z) + \Gamma_s\lambda_s\sigma_{as}P_s^+(z)}{\Gamma_p\lambda_p\sigma_p^{tot}P_p^{tot}(z) + \frac{hCA_{core}}{\tau} + \sum_j\Gamma_A\lambda_j\sigma_A^{tot}P_A^{tot}(z) + \Gamma_s\lambda_s\sigma_s^{tot}P_s^+(z)} \tag{26}$$

$$\pm\frac{dP_p^\pm(z)}{dz} = \pm\Gamma_p\left[\left(\sigma_p^{tot} - \sigma_{24}\right)N_2(z) - \sigma_{ap}N\right]P_p^\pm(z) \mp \alpha_p P_p^\pm(z) \tag{27}$$

$$\frac{dP_s^+(z)}{dz} = \Gamma_s(\lambda)\left[\sigma_s^{tot}N_2(z) - \sigma_{as}N\right]P_s^+(z) - \alpha_s P_s^+(z) \tag{28}$$

$$\begin{aligned}&\pm\frac{dP_A^\pm(z)}{dz} = \pm\Gamma_A\left[\sigma_A^{tot}N_2(z) - \sigma_{aA}N\right]P_A^\pm(z)\\ &\mp\alpha_A P_A^\pm(z) \pm \Gamma_A\sigma_{eA}N_2(z)P_0(\lambda) \pm S.\alpha_{RS}P_A^\mp(z)\end{aligned} \tag{29}$$

It is worth mentioning that there are no significant nonlinear optical effects such as SBS and SRS as well as thermal damages up to 50 W–CW single–mode pump powers [5]. In addition, the dipole–dipole interaction, clustering, and quenching are serious only in highly doping elements.

3.3. Gain saturation

Tremendous efforts were made to develop the fiber amplifiers during the recent decade. Indeed, the amplifier is characterized by very important and unique gain and saturation parameters [55–60] that are often used to analyze and compare different gain mediums in certain applications.

The advantages of operating in the gain saturation regime are mainly summarized as follows [4]:

1. Small fluctuations in the input signal do not reflect the same extent in the output amplified signal.
2. The fiber amplifier, which has multiple spectrally close input signals with varied intensity, may work as a gain equalizer because smaller input signal powers have higher gain (through less saturation), and higher input powers have lower gain (due to a higher degree of saturation).
3. A saturated optical amplifier demonstrates a high–energy extraction efficiency; therefore, the overall efficiency of the system is high.

According to theoretical analysis, high–input optical fluence does not increase indefinitely in an amplifier but rather saturates, leading to amplifier gain reduction. Obviously, even from the general consideration of energy conservation, the gain of the amplifier has to saturate, because one cannot extract more power from the amplifier than it was excited (pumped) with.

The emission and absorption cross sections are used to introduce the gain coefficient. According to Eq. (28), the gain for signal radiation after simplification can be defined as follows:

$$\gamma_s(z) = \Gamma_s\left[\sigma_{es}N_2(z) - \sigma_{as}N_1(z)\right] \tag{30}$$

In a fiber amplifier, it depends on the distance z from its input end. By substituting Eq. (26) into Eq. (30) and ignoring ASE noises, the gain is rearranged in the following formalism:

$$\gamma_s(z) = \frac{\left(hCA_{core}\right)^{-1}\Gamma_s\Gamma_p\lambda_p N\tau\left(\sigma_{ap}\sigma_{es} - \sigma_{ep}\sigma_{as}\right)P_p^{tot}(z) - N\Gamma_s\sigma_{as}}{\left(hCA_{core}\right)^{-1}\Gamma_p\lambda_p\tau\sigma_p^{tot}P_p^{tot}(z) + 1 + \left(hCA_{core}\right)^{-1}\Gamma_s\lambda_s\tau\sigma_s^{tot}P_s^{+}(z)} \tag{31}$$

Due to high signal power, which saturates the gain, the first term of the dominator is small enough with respect to others. Assuming $\sigma_{as} \ll \sigma_{es}$ in the numerator, $\gamma_s(z)$ is given by [5, 26]

$$\gamma_s(z) = \frac{\left(N\Gamma_p\sigma_{ap}\right)\left(\lambda_p/\lambda_s\right)\left[P_p^{tot}(z)/P_s^{sat}(z)\right] - N\Gamma_s\sigma_{as}}{1 + P_s^{+}(z)/P_s^{sat}(z)} \tag{32}$$

where the signal saturation power is introduced as follows:

$$P_s^{sat}(z) = \frac{hCA_{core}}{\Gamma_s\lambda_s\left(\sigma_{as} + \sigma_{es}\right)\tau} \tag{33}$$

It decreases the small–signal gain by a factor of one–half equivalent to a 3 dB reduction in gain [49]. It is worth mentioning that not only $P_s^{sat}(z)$ relies on the photon energy of the seed signal,

the mode field area, the upper state lifetime, the absorption, and stimulated emission cross sections of the gain media, but it also strongly correlates to the signal overlapping factor. Combining Eqs (11) and (33), we imply that $P_s^{sat}(z)$ is a linear function of pump and signal powers in CW regime, namely

$$P_s^{sat}(z) = \frac{hCA_{core}}{\lambda_s(\sigma_{as}+\sigma_{es})\tau}\frac{P^{core}+P^{clad}}{P^{core}} \tag{34}$$

From another point of view, the gain coefficient in the steady–state condition can be explained by

$$\gamma_s(z) = \frac{\gamma_0(z)}{1+P_s^+(z)/P_s^{sat}(z)} \tag{35}$$

where $\gamma_0(z)$ is the small–signal gain. The role of the term $P_s^+(z)/P_s^{sat}(z)$ is to reduce the gain as signal power increases in the fiber. This phenomenon is common to all amplifiers and is referred to as gain saturation. If the amplifier operates at power levels such that $P_s^+(z)/P_s^{sat}(z) \ll 1$ for all z, the amplifier is said to operate in the unsaturated regime. Moreover, by comparing Eqs (32) and (35), the theoretical term for the maximum value of the gain at distance z is given by [5, 26]

$$\gamma_0(z) = N\Gamma_p\sigma_{ap}(\lambda_p/\lambda_s)\left[P_p^{tot}(z)/P_s^{sat}(z)\right] - N\Gamma_s\sigma_{as} \tag{36}$$

Let us assume a doped dual–clad fiber amplifier with length L, such that pumping light is injected into the inner clad, and the laser seed is transmitted into the active medium. In strongly pumped single–pass fiber amplifier, $N_2(z)$ is presumed to be much smaller than N over a significant part of the cavity length, such that Eq. (27) becomes analytically integrable to yield the axial backward and forward propagation pump powers along the fiber core according to the Lambert–Beer (L–B) law:

$$P_p^{tot}(z) = P_p^+(z) + P_p^-(z) = P_p^+(0)e^{-\alpha z} + P_p^-(L)e^{\alpha(z-L)} \tag{37}$$

where $P_p^+(0)$ and $P_p^-(L)$ are the pump powers injected in both fiber ends at $z=0$ and $z=L$, respectively. In fact, the total attenuation α includes the scattering and pump absorption losses, namely

$$\alpha = \alpha_p + N\Gamma_p\sigma_{ap} \tag{38}$$

Here, α_p depicts the absorption coefficient of the core at the pump wavelength due to scattering loss. Taking average over the fiber length, the effective small–signal gain coefficient per unit length is written in terms of α consequently [56]:

$$\gamma_0 = \frac{1}{L}\int_0^L \gamma_0(z)dz \tag{39}$$

Hence

$$\gamma_0 = (1/L)(\lambda_p/\lambda_s)\left(1-\frac{\alpha_p}{\alpha}\right)\left(1-e^{-\alpha L}\right)\left(\frac{P_p^+(0)+P_p^-(L)}{P_s^{sat}}\right) - N\Gamma_s\sigma_{as} \tag{40}$$

In the general case of the varied inversion along the gain fiber, the absolute gain factor should be integrated along the entire fiber length [4]:

$$g = \exp\left(\int_0^L \gamma_0(z)dz\right) \tag{41}$$

Accordingly, the gain and saturation properties are strongly dependent on the pump power, dopant concentration, fiber length, as well as the pumping modes (co–/counter–propagation and bidirectional pumping) mainly due to the dominant effect of the filling factors [26, 61, 62].

In return, if optical pulses are amplified, the gain coefficient associates with the elapsed time t due to $N_2(z, t)$. Therefore, the gain can be expressed as follows:

$$\gamma_s(z) = \frac{\gamma_0(z)}{1+I_s^+(z)/I_s^{sat}(z)} \tag{42}$$

where $I_s^+(z)$ is the amplified light intensity, and $I_s^{sat}(z)$ is the so–called gain saturation parameter, defined as an intensity of the amplifying beam in active medium at which the small–signal (unsaturated) gain coefficient is reduced by 50% (i.e., half). In turn, the gain saturation parameter with good approximation can be clarified as the following general formula:

$$I_s^{sat}(z) = \frac{hC}{\Gamma_s\lambda_s(\sigma_{as}+\sigma_{es})\tau} \tag{43}$$

4. The spectral line broadening

The nature of spectral line broadening plays a very important role in the performance of the fiber laser amplifiers. The stimulated emission cross section is conventionally rewritten by

$$\sigma_e(\nu) = \frac{\lambda^2}{8\pi n^2 \tau} g(\nu) \tag{44}$$

where $g(\nu)$ indicates the spectral line shape. Using Eqs (33), (40), and (43), one can realize that the amplifying parameters, i.e., the small–signal gain and the saturation intensity/power are believed to be correlated to the line shape and the consequent broadened linewidth.

The spectral line broadening at room temperature (300 K) smooths the overall line shape, which becomes resolved only at low temperatures [4]. With a temperature decrease, Stark level structure becomes more and more evident and determines the line shape characteristic profile.

In the case of rare–earth–doped fiber oscillator and amplifier, different types of broadenings exist. These include strong homogeneous as well as the inhomogeneous broadenings [56, 63]. The designation of whether the transition line shape is homogeneously or inhomogeneously broadened is based on whether the lines are from the same type of centers or from different sorts.

Usually, a homogeneous broadening is explained by the random perturbation of a similar type of optical centers, while that from different kinds is responsible for inhomogeneously broadened lines [4]. Such kinds of interaction result in the shortening of the excited state lifetime of the optical center.

Therefore, the homogeneous broadening is inherent to each atom in a medium as depicted in Figure 3(a). It can be spontaneous broadening, Stark broadening, collision broadening, thermal and dipolar, and so on. The spontaneous broadening is a primary broadening yielded from the lifetime of a pumping level and the frequency uncertainty. The Stark broadening is due to the degeneration of energy level caused by external electric field, making the lifetime very short and the spectral width very large. Moreover, the collision broadening is dominant for gas lasers as excimer lasers operate with high gas pressure discharge.

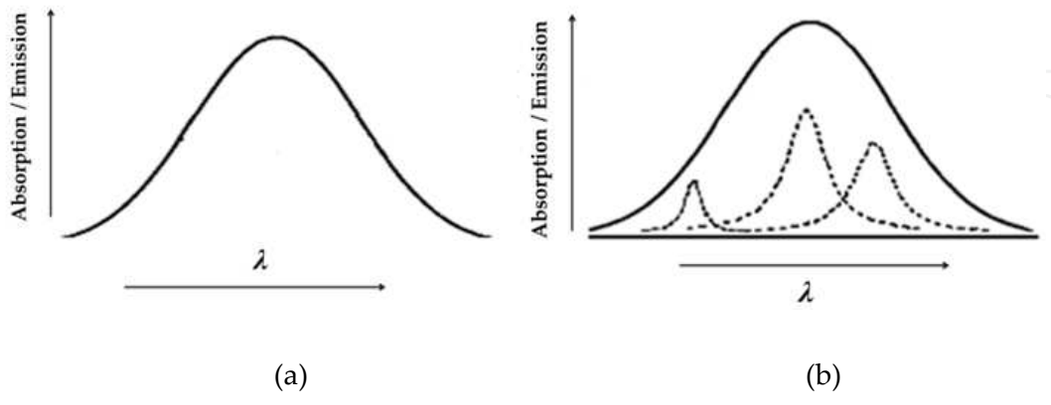

Figure 3. (a) Homogeneous and (b) inhomogeneous broadenings

Conversely, the inhomogeneous broadening of the optical center's line shape during a transition between energy levels originates from a local site–to–site variation in the optical

center's surrounding field in the lattice environment. The strength and symmetry of the field around the rare–earth ion determine the spectral properties of the optical transitions, as well as the transition strength. According to Figure 3(b), in the case of inhomogeneous broadening, the overall shape of the spectral line is a superposition of all individual, homogeneously broadened lines corresponding to different types of the optical centers. Hence, this is a phenomenon that various frequencies are generated by a variety of influences, and the spectrum is broadened.

The inhomogeneous broadening can be a strain caused by lattice defect or inhomogeneity of magnetic or electric field (crystalline field) for solid–state lasers and Doppler broadening for gas lasers.

In a crystal of solid–state laser, the crystalline field is not uniform since the crystal is imperfect. As a result, a large inhomogeneous broadening is yielded. In a glass doped with rare–earth ions, the inhomogeneous width is relatively largely broadened compared with the crystalline solid–state laser. The amorphous nature of the glass, random distribution of dopants, and host material imperfection lead to site–to–site variations of the local electric field, producing a degree of inhomogeneous broadening in the system which results in spectral hole burning (SHB).

Indeed, the optical transition line shape in the case of homogeneous broadening is described by a Lorentzian function given by

$$g_{\mathrm{L}}(\nu)=\frac{1}{2\pi^2}\frac{(\Delta\nu_{\mathrm{h}}/2)}{(\nu_{\mathrm{h}}-\nu_0)^2+(\Delta\nu_{\mathrm{h}}/2)^2} \tag{45}$$

where ν_0 is the central frequency of the optical transition, and $\Delta\nu_{\mathrm{h}}$ represents the transition spectral line full width at half maximum (FWHM) as well as $\int_{-\infty}^{+\infty} g_{\mathrm{L}}(\nu,\nu_0)d\nu=1$. Figure 4 shows Lorentzian/Gaussian function in the case of homogeneous/inhomogeneous broadening.

Subsequently, the line shape of the inhomogeneously broadened optical transition corresponds to the Gaussian line profile, which can be expressed as the following function of frequency:

$$g_{\mathrm{G}}(\nu)=\frac{2}{\Delta\nu_{\mathrm{inh}}}\sqrt{\frac{\ln 2}{\pi}}\exp\left[-\ln 2\left(\frac{\nu_{\mathrm{inh}}-\nu_0}{\Delta\nu_{\mathrm{inh}}/2}\right)^2\right]\frac{(\Delta\nu_{\mathrm{h}}/2)}{(\nu-\nu_0)^2+(\Delta\nu_{\mathrm{h}}/2)^2} \tag{46}$$

where $\Delta\nu_{\mathrm{inh}}$ is the FWHM of the inhomogeneously broadened line. Concluded by the optical center surrounding fields, the inhomogeneous linewidth is insensitive to the temperature of the host material.

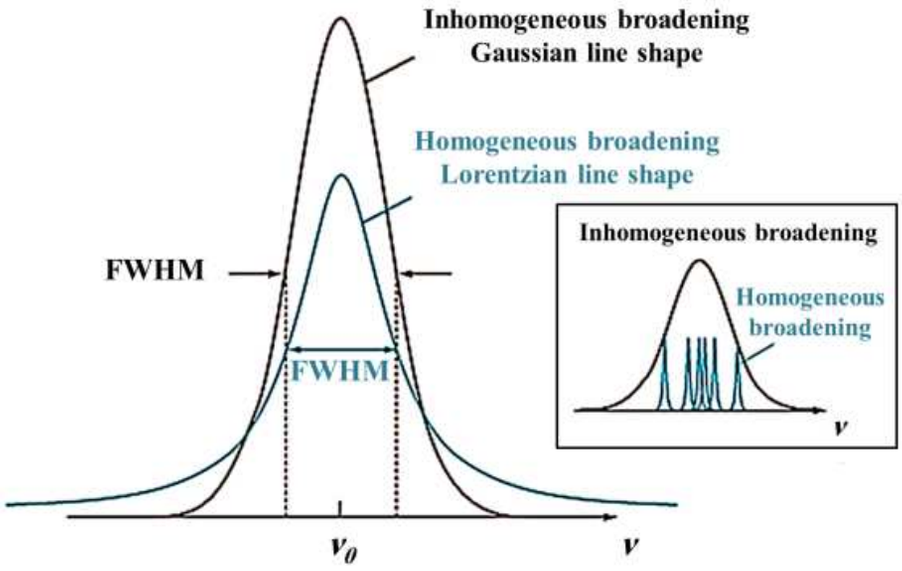

Figure 4. Lorentzian–shaped and Gaussian–shaped spectra [64]

5. Amplification relations

The state–of–the–art fiber amplifiers are significantly related to the determination of amplifying parameters (gain and saturation) which are not explicitly introduced into the rate equations; however, these can be obtained by using a suitable amplification relation. It is applicable for the homogeneous line broadening in Yb:silica fiber amplifiers [63] as well as the Er–doped silica fiber lasers with inhomogeneous line broadening.

In general, the laser amplification consists of a couple of distinct transient (short pulse) and steady–state (long pulse) regimes. The gain and saturation values can be estimated by numerically solving the amplification relations performing the best fitting based on least square method (LSM).

5.1. Pulsed regime

In the transient form of the amplification relation, the input pulse is considerably shorter than the fluorescence lifetime of the medium, such as Q–switched or mode–locked pulses with inhomogeneous gain media. The propagation rate equations are the best procedure to simulate the amplified signal energy released from the stimulated emission. This process depends on the energy stored in the upper laser level prior to the synchronization situation of the pumped atoms and incident seed signal. Furthermore, the time–dependent photon transport equation can be utilized to evaluate how an inverted population affects the distribution of a pulse traversing through the amplifier. Hopf [65] and Frontz–Nodvik [66] solved the nonlinear equations for various types of input pulse shapes to obtain the inverted electron population and the photon flux, while the input signal to the amplifier was taken as a square pulse of duration τ. Finally, the transient amplification relation is given by

$$E_{out} = E_s^{sat} \ln\left\{1 + \left[\exp\left(\frac{E_{in}}{E_s^{sat}}\right) - 1\right]\exp\left(\gamma_0 L\right)\right\} \tag{47}$$

where E_{in} and E_{out} denote the input and output signal energy and E_s^{sat} the saturation energy derived from the instantaneous rate equations of the optical pulse, respectively.

For the pulses whose shapes are sufficiently near the eigen–function for the propagation in the amplifying medium, the change in the average temporal width of the pulse can be reasonably expected to be negligible. In such cases, the approximation $E_n = \tau \times \boldsymbol{I}_{\mathbf{n}}$ is justified where n can be designated as input, output, or saturation. With this substitution, Eq. (47) can be rewritten as [59]

$$\boldsymbol{I}_{\mathbf{out}} = \boldsymbol{I}_{\mathbf{s}}^{\mathbf{sat}} \ln\left\{1 + \left[\exp\left(\frac{I_{in}}{I_s^{sat}}\right) - 1\right]\exp\left(\gamma_0 L\right)\right\} \tag{48}$$

where $\boldsymbol{I}_s^{sat}$, is the effective saturation intensity:

$$\boldsymbol{I}_{\mathbf{s}}^{\mathbf{sat}} = \frac{t_2}{2\tau} I_s^{sat} \tag{49}$$

Here, t_2 is the upper level lifetime of the transition.

5.2. CW regime

For the seed signal, which is long compared to the fluorescent time including the free running oscillator or the CW seed laser [5, 67, 68] under homogeneous line broadening, a Hargrove [69] steady–state gain characterizes the amplification mechanism as follows [5, 6]:

$$-\ln\left(P_{out} / P_{in}\right) = \frac{P_{out} - P_{in}}{P_s^{sat}} - \gamma_0 L \tag{50}$$

Here, P_{in} (P_{out}) represents the input (output) signal power to the amplifier. This equation can be simplified using mathematical derivations such that [70]

$$P_{out} = P_s^{sat} \times W\left[\frac{P_{in}\exp\left(\gamma_0 L + \frac{P_{in}}{P_s^{sat}}\right)}{P_s^{sat}}\right] \tag{51}$$

where W shows the Lambert W –Function to be defined by the series expansion [71]:

$$W(x)=\sum_{n=1}^{\infty}\frac{(-1)^{n-1}n^{n-2}}{(n-1)!}x^{n} \tag{52}$$

In addition, in the limiting cases

$$P_{\text{out}}=P_{\text{in}}\exp(\gamma_0 L) \qquad P_{\text{in}}\ll P_{\text{s}}^{\text{sat}} \tag{53}$$

$$P_{\text{out}}=P_{\text{in}}+P_{\text{s}}^{\text{sat}}\gamma_0 L \qquad P_{\text{in}}\gg P_{\text{s}}^{\text{sat}} \tag{54}$$

These relations indicate that for low–input powers, the overall gain ($G=P_{\text{out}}/P_{\text{in}}$) is nonlinearly proportional to gain–length product, and the gain coefficient becomes equal to the small–signal gain. In contrast, the gain reduces to the saturated value for the high–input signals.

A straightforward integration shows that the CW gain of the amplifier is considered by

$$G(\nu)=\exp\left[\int_0^L g(z,\nu)dz\right] \tag{55}$$

The origin of gain saturation lies in the power dependence of the gain coefficient. Since $g(z, \nu)$ is diminished when P_{in} becomes comparable to $P_{\text{s}}^{\text{sat}}$, the amplification factor G is also expected to decrease.

Author details

Maryam Eilchi[1*] and Parviz Parvin[2]

1 Laser and Optics Research Institute, Nuclear Science and Technology Research Institute, Tehran, Iran

2 Photonic Engineering Group, Department of Physics, Amirkabir University of Technology, Tehran, Iran

References

[1] F. J. Duarte. Tunable laser applications. 2nd ed. CRC Press. Taylor & Francis group, LLC; 2008. 480p.

[2] C. Labaune, D. Hulin, A. Galvanauskas, and G. A. Mourou. On the feasibility of a fiber-based inertial fusion laser driver. Optics Communications. 2008; 281(15–16): 4075–4080.

[3] G. Mourou, B. Brocklesby, T. Tajima, and J. Limpert. The future is fibre accelerators. Nature Photonics. 2013; 7: 258–261.

[4] Valerii (Vartan) Ter-Mikirtychev. Fundamentals of Fiber Lasers and Fiber Amplifiers. Switzerland: Springer International Publishing; 2014.

[5] N. S. Kim, T. Hamada, M. Prabhu, C. Li, J. Song, K. Ueda, A. Liu, and H. J. Kong. Numerical analysis and experimental results of output performance for Nd-doped double-clad fiber lasers. Optics communications. 2000; 180: 329–337.

[6] H. M. Pask, R. J. Carman, D. C. Hanna, A. C. Tropper, C. J. Mackechnie, P. R. Barber, and J. M. Dawes. Ytterbium-doped silica fiber lasers: versatile sources for the 1-1.2 μm region. IEEE Journal of Selected Topics in Quantum Electronics. 1995; 1: 2–13.

[7] Y. Feng, S. Huang, A. Shirakawa, and K. Ueda. 589nm light source based on Raman fiber laser. Japanese Journal of Applied Physics.2004; 43(6A): L722–L724.

[8] D. Georgiev, V. P. Gapontsev, A. G. Dronov, M. Y. Vyatkin, A. B. Rulkov, S. V. Popov, and J. R. Taylor. Watts-level frequency doubling of a narrow line linearly polarized Raman fiber laser to 589nm. Optics Express. 2005; 13(18): 6772–6776.

[9] D. Bonaccini Calia, W. Hackenberg, S. Chernikov, Y. Feng, and L. Taylor. AFIRE: fiber Raman laser for laser guide star adaptive optics. In: Proceedings of SPIE 6272, 62721M; 2006.

[10] P. Dupriez, C. Farrell, M. Ibsen, J. K. Sahu, J. Kim, C. Codemard, Y. Jeong, D. J. Richardson, and J. Nilsson. 1W average power at 589 nm from a frequency doubled pulsed Raman fiber MOPA system. In: Proceedings of SPIE 6102, 61021G; 2006.

[11] Y. Feng, L. Taylor, and D. Bonaccini Calia. Multiwatts narrow linewidth fiber Raman amplifiers. Optics Express. 2008; 16(15): 10927–10932.

[12] Y. Feng, L. Taylor, and D. Bonaccini Calia. 20W CW, 4MHz linewidth Raman fiber amplifier with SHG to 589nm. In: Photonics West; Proceedings of SPIE 7195, xvii–xviii; 2009.

[13] L. Taylor, Y. Feng, and D. B. Calia. High power narrowband 589 nm frequency doubled fibre laser source. Optics Express. 2009; 17(17):14687–14693.

[14] J. H. Franz, V. K. Jain. Optical Communications: Components and Systems. CRC Press. Narosa Publishing House; 2000. 717p.

[15] J. Hansryd and P. A. Andrekson. Broad-band continuous-wave-pumped fiber optical parametric amplifier with 49-dB gain and wavelength-conversion efficiency. IEEE Photonics Technology Letters. 2001; 13: 194–196.

[16] J. Hansryd, P. A. Andrekson, M. Westlund, J. Li, and P. O. Hedekvist. Fiber-based optical parametric amplifiers and their applications. IEEE Journal of Selected Topics in Quantum Electronics. 2002; 8(3).

[17] O. G. Okhotnikov. Fiber Lasers. Wiley-VCH Verlag GmbH & Co. KGaA; 2012. 294p.

[18] D. E. McCumber. Theory of phonon-terminated optical masers. Physical Review. 1964; 134: A299–A306.

[19] W. J. Miniscalco and R. S. Quimby. General procedure for the analysis of Er^{3+} cross-section. Optics Letters. 1991; 16: 258–260.

[20] H. M. Pask, R. J. Carman, D. C. Hanna, A. C. Tropper, C. J. Mackechnie, P. R. Barber and J. M. Dawes. Ytterbium–doped silica fiber lasers: Versatile sources for the 1~1.2μm region. IEEE Journal of Selected Topics in Quantum Electronics.1995; 1: 2–13.

[21] M. R. A. Moghaddam, S. W. Harun and H. Ahmad. Comparison between Analytical Solution and Experimental Setup of a Short Long Ytterbium Doped Fiber Laser. Optics and Photonics Journal.2012; 2(2): 65–72.

[22] M. Premaratne and G. P. Agrawal. Light Propagation in Gain Media, Optical Amplifiers. Cambridge: Cambridge University Press; 2011.

[23] L. Pan, I. Utkin, and R. Fedosejevs. Experiment and numerical modeling of high-power passively Q-switched ytterbium-doped double-clad fiber lasers. IEEE Journal of Quantum Electronics. 2010; 46: 68–75.

[24] Z. Duan, L. Zhang, and J. Chen. Analytical solutions to rate equations including losses describing threshold pumped fiber lasers. Optik-International Journal for Light and Electron Optics. 2008; 119: 395–399.

[25] M. Gong, Y. Yuan, C. Li, P. Yan, H. Zhang, and S. Liao. Numerical modeling of transverse mode competition in strongly pumped multimode fiber lasers and amplifiers. Optics Express. 2007; 15: 3236–3246.

[26] M. Eichhorn. Numerical modeling of Tm-doped double-clad fluoride fiber amplifiers. IEEE Journal of Quantum Electronics. 2005; 41: 1574–1581.

[27] G. Hu, C. Shan, X. Deng, J. Zhang, Y. Pan, and L. Wang. Threshold characteristics of linear cavity Yb^{3+}-doped double-clad fiber laser. Optics & Laser Technology. 2005; 37: 3–7.

[28] L. Xiao, P. Yan, M. Gong, W. Wei, and P. Ou. An approximate analytic solution of strongly pumped Yb-doped double-clad fiber lasers without neglecting the scattering loss. Optics Communications. 2004; 230: 401–410.

[29] C. Jiang, W. Hu, and Q. Zeng. Numerical analysis of concentration quenching model of Er^{3+}-doped phosphate fiber amplifier. IEEE Journal of Quantum Electronics. 2003; 39: 1266–1271.

[30] I. Kelson and A. Hardy. Optimization of strongly pumped fiber lasers. Journal of Lightwave Technology.1999; 17: 891–897.

[31] I. Kelson and A. A. Hardy. Strongly pumped fiber lasers. IEEE Journal of Quantum Electronics. 1998; 34: 1570–1577.

[32] M. J. F. Digonnet. Rare-Earth-Doped Fiber Lasers and Amplifiers. 2nd ed. CRC Press. Marcel Dekker, Inc; 2001. 798p.

[33] R. Oron and A. Hardy. Approximate analytical expressions for signal amplification in strongly pumped fiber amplifiers. IEEE Proceedings of Optoelectronics. 1998; 145(2): 138–140.

[34] M. Ilchi-Ghazaani and P. Parvin. Impact of cavity loss on the performance of a single-mode Yb:silica MOFPA array. Optics & Laser Technology. 2015; 65: 94–105.

[35] N. A. Brilliant. Ytterbium-Doped, Dual-Clad Fiber Amplifiers. PhD Thesis, University of Mexico. 2001.

[36] M. Federighi and F. Di Pasquale. The effect of pair-induced energy transfer on the performance of silica fiber amplifiers with high Er^{3+}/Yb^{3+} concentrations. IEEE Photonics Technology Letters. 1995; 7(3): 303–305.

[37] A. Hardy and R. Oron. Signal Amplification in strongly pumped fiber amplifiers. IEEE Journal of Quantum Electronics. 1997; 33: 307–313.

[38] Y. Yuan, M. Gong, C. Li, and P. Yan. Theoretical and experimental study on transverse mode competition in a partial-coiled multimode fiber laser. Laser Physics. 2008; 18: 52–57.

[39] M. Iilchi-Ghazaani, P. Parvin, and S. Mohammadian. Determination of amplifying parameters of LMA Yb:silica fiber amplifier. In: 2013; Czech Republic. Proceedings of SPIE 8781, Integrated Optics: Physics and Simulations. 878116; 2013.

[40] P. C. Becker, A. Lidgard, J. R. Simpson, and N. A. Olsson. Erbium-doped fiber amplifier pumped in the 950-1000 nm region. IEEE Photonics Technology Letters. 1990; 2(1): 35–37.

[41] Z. Duan, J. Chen, Z. Gao, and Y. Huang. Theoretical analysis of multimode fiber amplifiers and lasers containing spatial filters. Optik-International Journal for Light and Electron Optics. 2011; 122(24): 2211–2215.

[42] M. A. Rebolledo and S. Jarabo. Erbium-doped silica fiber modeling with overlapping factors. Applied Optics. 1994; 33(24): 5585–5593.

[43] D. Gloge. Weakly Guiding Fibers. Applied Optics. 1971; 10(10): 2252–2258.

[44] A. D'Orazio, M. De Sario, L. Mescia, V. Petruzzelli, and F. Prudenzano. Refinement of Er^{3+}-doped hole-assisted optical fiber amplifier. Optics Express. 2005; 13: 9970–9981.

[45] T. J. Whitley and R. Wyatt. Alternative Gaussian spot size polynomial for use with doped fiber amplifiers. IEEE Journal of Photonics Technology Letters. 1993; 5(11): 1325–1327.

[46] P. Myslinski and J. Chrostowski. Gaussian-mode radius polynomials for modeling doped fiber amplifiers and lasers. Microwave and Optical Technology Letters. 1996; 11: 61–64.

[47] E. Desurvire and J. R. Simpson. Amplification of spontaneous emission in erbium-doped single-mode fibers. IEEE Journal of Lightwave Technology. 1989; 7: 835–845.

[48] M. N. Zervas and R. I. Laming. Rayleigh scattering effect on the gain efficiency and noise of erbium-doped fiber amplifiers. IEEE Journal of Quantum Electronics. 1995; 31: 468–471.

[49] A. A. Hardy and R. Oron. Amplified spontaneous emission and Rayleigh backscattering in strongly pumped fiber amplifiers. Journal of Lightwave Technology. 1998; 16: 1865–1873.

[50] Q. Han, J. Ning, H. Zhang, and Z. Chen. Novel shooting algorithm for highly efficient analysis of fiber Raman amplifiers. Journal of Lightwave Technology. 2006; 24: 1946–1952.

[51] A. H. Hartog and M. P. Gold. On the theory of backscattering in single-mode optical fibers. Journal of Lightwave Technology. 1984; LT-2: 76–82.

[52] E. G. Neumann. Single Mode Fibers Fundamentals. New York: Springer-Verlag; 1988.

[53] R. Oron and A. A. Hardy. Rayleigh backscattering and amplified spontaneous emission in high-power ytterbium-doped fiber amplifiers. JOSA B. 1999; 16: 695–701.

[54] P. C. Becker, N. A. Olsson, and J. R. Simpson. Erbium-Doped Fiber Amplifiers: Fundamentals and Technology. New York: Lucent Technologies; 1999.

[55] S. Mohammadian, P. Parvin, M. Ilchi-Ghazaani, R. Poozesh, and K. Hejaz. Measurement of gain and saturation parameters of a single-mode Yb:silica fiber amplifier. Optical Fiber Technology. 2013; 19: 446–455.

[56] P. Parvin, M. Ilchi-Ghazaani, A. Bananej, and Z. Lali-Dastjerdi. Small signal gain and saturation intensity of a Yb: Silica fiber MOPA system. Optics & Laser Technology. 2009; 41(7): 885–891.

[57] S. Behrouzinia, R. Sadighi-Bonabi, P. Parvin, and M. Zand. Temperature dependence of the amplifying parameters of a copper vapor laser. Laser Physics - Lawrence. 2004; 14(8): 1050–1053.

[58] S. Behrouzinia, R. Sadighi, and P. Parvin. Pressure dependence of the small-signal gain and saturation intensity of a copper vapor laser. Applied Optics. 2003; 42(6): 1013–1018.

[59] P. Parvin, M. S. Zaeferani, K. Mirabbaszadeh, and R. Sadighi. Measurement of the small-signal gain and saturation intensity of a XeF discharge laser. Applied Optics. 1997; 36(6): 1139–1142.

[60] A. Saliminia, P. Parvin, A. Zare, and R. Sadighi. The small signal gain and the saturation intensity measurement of the nitrogen-ion laser. Optics & Laser Technology. 1996; 28(3): 207–211.

[61] A. Escuer, S. Jarabo, and J.M. Alvarez. Analysis of theoretical models for erbium-doped silica fibre lasers. Optics Communications. 2001; 187: 107–123.

[62] M. A. Rebolledo and S. Jarabo. Erbium-doped silica fiber modelling with overlapping factors. Applied Optics. 1994; 33: 5585–5593.

[63] R. Paschotta, J. Nilsson, A. C. Tropper, and D. C. Hanna. Ytterbium-doped fiber amplifiers. IEEE Journal of Quantum Electronics. 1997; 33(7): 1049–1056.

[64] Laser Tutorial. Kokyo Inc; 2014–2015. Available from: http://laser.photoniction.com/tutorial/

[65] F. Hopf. High Energy Lasers and Their Applications. Addison: Wesley; 1974.

[66] L. M. Frantz, J. S. Nodvik. Theory of pulse propagation in a laser amplifier. Journal of Applied Physics.1963; 34: 2346–2349.

[67] A. A. Hardy, R. Oron. Signal amplification in strongly pumped fiber amplifiers. IEEE Journal of Quantum Electronics.1997; 33: 307–313.

[68] I. Kelson, A. Hardy. Strongly pumped fiber lasers. IEEE Journal of Quantum Electronics.1998; 34: 1570–1577.

[69] W. Koechner. Solid-State Laser Engineering. Springer-Verlag New York; 2006. 748p.

[70] O. Mahran. Gain and noise figure of ytterbium doped lead fluoroborate optical fiber Amplifiers. Australian Journal of Basic and Applied Sciences. 2010; 4(8): 4020–4028.

[71] R. M. Corless, G. H. Gonnet, D. E. G. Hare, D. J. Jeffrey, and D. E. Knuth. On the Lambert W function. Advances in Computational Mathematics. 1996; 5(1): 329–359.